

The onset, extent and duration of dehydration in the Southern Hemisphere polar vortex

Elizabeth M. Stone, Azadeh Tabazadeh and Eric Jensen
NASA Ames Research Center, Moffett Field, California

Hugh C. Pumphrey
Department of Meteorology, University of Edinburgh, UK

Michelle L. Santee
Jet Propulsion Laboratory, California Institute of Technology, Pasadena,
California

John L. Mergenthaler
Lockheed Martin Advanced Technology Center, Palo Alto, California

Short title: DEHYDRATION IN THE SH POLAR VORTEX

Abstract.

Satellite observations of water vapor and aerosol extinction along with temperature trajectory calculations are analyzed for the Southern Hemisphere winter of 1992 in order to determine the onset, extent and duration of dehydration within the polar vortex. Our investigation uses measurements of water vapor from the Microwave Limb Sounder (MLS) and aerosol extinction from the Cryogenic Limb Array Etalon Spectrometer (CLAES), both onboard the Upper Atmosphere Research Satellite (UARS). Evidence of persistent ice cloud formation, supported by temperature statistics obtained from air parcel trajectories, suggest that the onset of the dehydration process, occurs between late June and early July. By late August-early September water vapor depleted areas within the vortex no longer coincide with high aerosol extinctions, indicating that severe dehydration has occurred with the irreversible removal of water vapor over vast areas. Areas with depleted levels of water vapor, below the pre-winter values, persist well into November. Evidence for dehydration is found on potential temperature surfaces from 420 K (the lower limit of the MLS measurements) to 520 K (approximately 16 to 22 km). The horizontal extent of the dehydrated area at 465 K encompasses up to 35% of the total vortex area equatorward of 80°S. A comparison of CLAES aerosol extinction measurements and model calculations of aerosol extinction suggests an average ice particle number concentration and size of 10^{-2} - 10^{-3} cm^{-3} and 10-30 μm , respectively. We show that the difference between the timing of the onset of dehydration found here and that in a recent analysis of Polar Ozone and Aerosol Measurement III (POAM) observations can be explained by the latitudinal sampling pattern of the POAM instrument.

1. Introduction

Polar stratospheric clouds (PSCs) form at low temperatures in the winter polar vortex and have a direct influence on atmospheric chemistry by their involvement in heterogeneous ozone chemistry [Solomon, 1999]. PSCs also act as sinks for gas phase water vapor and nitric acid resulting in stratospheric dehydration [e.g., Kelly *et al.*, 1989; Hofmann and Deshler, 1991; Nedoluha *et al.*, 2000] and denitrification [e.g., Toon *et al.*, 1986; Santee *et al.*, 1999; Tabazadeh *et al.*, 2000a].

Understanding the physical properties of the clouds and the meteorological conditions under which they form is important for studies of the polar vortex. Particle size and composition influence the optical properties of the clouds, which affect remote sensing [Toon *et al.*, 1990; Browell *et al.*, 1990]; composition of the aerosols impacts constituent budgets and chemical reactions [Solomon, 1999]; and chemical processes which are dependent upon relative humidity will be affected by the deficit of water vapor due to dehydration [Hanson *et al.*, 1994]. PSCs are separated into two types [WMO, 1999]. Type II PSCs are composed of water ice and form at temperatures below the ice frost point. Type I clouds form at temperatures above the ice frost point and consist of both liquid and solid nitric acid-containing cloud particles. Our study examines the timing and extent of dehydration that occurs as a result of ice particle nucleation, growth and sedimentation, a process that irreversibly removes water vapor from the stratosphere.

The Airborne Antarctic Ozone Experiment (AAOE) in August-September 1987 showed the first evidence of stratospheric dehydration in the Antarctic vortex [Kelly *et al.*, 1989], an observation that was extended vertically by balloon profiles from the Antarctic continent [Hofmann *et al.*, 1991; Rosen *et al.*, 1988; Vömel *et al.*, 1995]. Using balloon measurements over McMurdo in 1994, Vömel *et al.* [1995] conclude that dehydration starts around mid June and persists into November. However, only a limited number of *in situ* measurements have been made over the Antarctic region over the course of several winters. Satellite observations can provide a more extensive view of the polar regions. Springtime dehydration has been

noted in the analysis of Halogen Occultation Experiment (HALOE) data [*Pierce et al.*, 1994; *Rosenlof et al.*, 1997]. *Santee et al.* [1995] report on the interhemispheric differences in wintertime water vapor from the Microwave Limb Sounder (MLS) and *Ricaud et al.* [1995] deduce PSCs from MLS water vapor and Cryogenic Limb Array Etalon Spectrometer (CLAES) aerosol extinction measurements from several days in August-September 1992. Evidence for wintertime dehydration is also found in measurements from the Atmospheric Trace Molecule Spectroscopy (ATMOS) instrument [*Manney et al.*, 1999], and *Nedoluha et al.* [2000] report on Polar Ozone and Aerosol Measurement III (POAM) observations which show dehydration occurring in the Southern Hemisphere (SH) winter of 1998.

We examine near-coincident UARS satellite measurements of stratospheric water vapor and aerosol extinction in the SH winter polar region to identify the onset, extent and duration of dehydration in 1992. We correlate water vapor mixing ratios with aerosol extinction and use temperature statistics obtained from air parcel trajectories to deduce where and when the dehydration process occurs. The onset of dehydration is identified by early signs of persistent ice cloud formation. At the onset, areas showing the depletion of water vapor coincide with areas of high aerosol extinction. Severe dehydration has occurred when areas of low water vapor no longer coincide with areas of high aerosol extinction, indicating that water vapor has been removed irreversibly from the atmosphere. We compare measured and calculated aerosol extinction to infer ice particle size and number density in the dehydration path.

2. Observations

Water vapor data for this study come from the MLS instrument onboard the Upper Atmosphere Research Satellite (UARS). We use the prototype water vapor product (version 104) described by *Pumphrey* [1999], which gives mixing ratios in the stratosphere from 0.1 to 100 hPa with a vertical resolution of 3-4 km. Although this is not an official UARS project MLS product, its validity and usefulness in scientific studies has been demonstrated [*Pumphrey et al.*, 2000; *Pumphrey*, 1999; *Manney et al.*, 1998]. MLS version 5 water vapor

has recently become available but we have chosen not to use it for this study because of systematic errors in the lower stratospheric data [Pumphrey *et al.*, 2000]. These measurements are available from September 1991 to April 1993, which includes only one SH winter.

The CLAES instrument, also onboard UARS, measures aerosol extinction coefficients [Mergenthaler *et al.*, 1997] which have been used to identify PSCs [Mergenthaler *et al.*, 1997; Ricaud *et al.*, 1995; Massie *et al.*, 1994] and to determine volume and surface area densities of type I PSCs [Massie *et al.*, 1997, 1998]. In identifying PSCs, aerosol extinction values are generally used qualitatively and threshold values for PSCs, depending on pressure, are determined relative to temperature and pre-winter observations. No information on particle size and concentration is given with the aerosol extinction data product. CLAES was operational from September 1991 until May 1993. Our analysis uses the CLAES version 8 aerosol extinction coefficients at 780 cm^{-1} .

MLS and CLAES measurements are nearly coincident in time and space, each with a horizontal resolution of $\sim 400 \text{ km}$. The vertical profiles of water vapor and aerosol extinction have been interpolated from the standard UARS grid to potential temperature surfaces using United Kingdom Meteorological Office (UKMO) temperatures. UKMO temperatures are also used for the analysis in sections 2 and 3. Comparisons of the UKMO temperatures with radiosonde observations show that systematic biases are less than $\sim 1 \text{ K}$ throughout the 1992 SH winter [Manney *et al.*, 1996].

We focus on the UARS SH viewing periods for one year, starting in April 1992 (1-30 April 1992, 2 June-12 July 1992, 14 August-20 September 1992, 30 October-28 November 1992, 10 January-8 February 1993, and 20 March-1 April 1993). We note that there are significant data gaps in the June-July viewing period due to problems with the UARS solar array which required the MLS and CLAES instruments to be turned off. Data availability limits this study to only one SH winter and we therefore do not assess year-to-year variability of dehydration. Although the SH winter of 1992 was not necessarily a typical year since there were high levels of stratospheric aerosol from Pinatubo, the duration of cold temperatures

and minimum temperatures were typical of wintertime conditions [WMO, 1999] (also see http://hyperion.gsfc.nasa.gov/Data_services/met/ann_data.html).

The water vapor annual cycles on potential temperature surfaces, compiled from the high-latitude MLS data, are shown in Figure 1. Daily averages are from data in the 70° S–80° S latitude range for one year starting in April 1992. The 420 K potential temperature level is at an altitude below 100 hPa in January through March, resulting in a lack of observations on that surface during that time. Potential temperature surfaces from 420 to 585 K show a minimum in water vapor in the winter months. These potential temperature surfaces cover pressure levels of 100 to 15 hPa. Since the water vapor data set does not extend below 100 hPa, we cannot observe the lower altitude limit of the dehydration. *Nedoluha et al.* [2000] show evidence for dehydration down to 12 km (or 360 K). At the higher potential temperature surfaces shown in Figure 1, the maximum in the annual cycle is found in winter (July-September). This study focuses on the wintertime values at and below 585 K.

The daily averages of aerosol extinction from CLAES are also shown in Figure 1. High extinctions are seen from mid June through late August from 420 to 585 K, in general coinciding with low values of water vapor (*i.e.* the deficit in gas phase water coincides with the presence of PSCs). Extinction values in September are lower than the pre-winter values. This feature in the annual development of extinction has been seen in other observations and is due to the cleansing of the atmosphere by the subsidence of PSCs and by descent in the vortex [Kent *et al.*, 1985; Thomason and Poole, 1993; Randall *et al.*, 1996; Nedoluha *et al.*, 2000]. Further, the Antarctic vortex is isolated in the winter and early spring [Bowman, 1993] so the observed changes in water vapor and aerosol extinction discussed here are not due to transport and mixing of air from outside the vortex.

Due to limited MLS water vapor measurements in late June and early July, we cannot observe the precise onset of dehydration. The measurements indicate that dehydration begins sometime after June 18. Extinction values are already high prior to June 18 due to Type I PSCs [Tabazadeh *et al.*, 2000a], which form at temperatures higher than the ice frost point.

A deficit in the water vapor mixing ratio is clearly seen on July 10-12 from 420 to 585 K. At 465 K, daily average values have dropped from 4 ppmv in mid June to 2.7 ppmv on July 10, suggesting that the onset of substantial dehydration could have occurred sometime after mid June and before 10 July. Water vapor values at the 420 K and 465 K levels drop further between mid July and early August when the next observation period begins. In August-September, daily mean values are between 2.3 and 2.8 ppmv at 465 K. Extinction values are still elevated in mid August but have diminished by early September. Measurements on the 585 K surface show a drop in the water vapor and an elevation of extinction in mid July, but values have recovered by August, indicating that the initial drop in water vapor seen at this level was reversible or that mixing ratios are replenished by the descent of moister air from above.

Figure 1 depicts only daily averages in the 70°S–80°S latitude range. Additional information can be found in the distributions of water vapor and aerosol extinction measurements. Figure 2 shows distributions of water vapor and aerosol extinction in the region of 50°S–80°S for different temperature bins ($T < 185$ K, $185 < T < 188$ K, $188 < T < 195$ K, and $195 < T < 210$ K (points with temperatures greater than 210 K are excluded)). We also show the distributions of water vapor and aerosol extinction for the 70°S–80°S latitude bin (for all temperatures). The $T < 185$ K bin represents air below the ice nucleation point (typically 3-4 K below the frost point [Tabazadeh *et al.*, 2000b; Chang *et al.*, 1999]) and the $185 < T < 188$ K bin represents observations between the frost point and the nucleation point. The $188 < T < 195$ K range is included because type I PSCs form at these temperatures. The distributions for data taken between April and November 1992 are separated according to the UARS yaw cycle.

We use the high latitude April measurements, representing pre-wintertime observations, and the June-July distributions to define representative values of low water vapor and high aerosol extinction. The water vapor distribution peaks at 4.3 ppmv in April and all the aerosol extinction values in this month are less than 0.0009 km^{-1} . In June–July, the mode of the water vapor distribution for $T < 185$ K is 2.3 ppmv and the $185 < T < 188$ K observations have two

peaks at 2.3 ppmv and near 4 ppmv. For $T > 188$ K the distributions are centered at 4 ppmv and fewer than 10% of the observations are less than 3.5 ppmv, indicating that in June–July the water vapor depleted area has not yet spread outside the regions with temperatures below the ice frost point. Therefore, we define dry areas to have water vapor mixing ratios less than 3.0 ppmv based on the April and June–July measurements. The areas of “high” aerosol extinction are identified by measurements which exceed 0.001 km^{-1} . The aerosol extinction threshold is slightly higher than the value used to identify PSCs at 46 hPa (0.00075 km^{-1}) by *Mergenthaler et al.* [1997]. Aerosol extinction values over 0.002 km^{-1} have large uncertainties due to the high optical depth of the PSCs along the limb viewing path [*Mergenthaler et al.*, 1997]. However, the uncertainties do not affect the classification of “high” aerosol extinction areas. The June–July distributions show that nearly all the observations which coincide with temperatures below 185 K have depleted water vapor amounts. 25% of the observations with $185 < T < 188$ K coincide with mixing ratios less than 3.0 ppmv. For temperatures above 188 K, there is no evidence of significant depletion of the water vapor.

The aerosol extinction distributions for the June–July observation period show evidence of both Type I and Type II PSCs. The temperature bins with $T < 195$ K all show observations of aerosol extinction above the April distributions. For the $185 < T < 188$ K temperature bin, 75% of the observations have aerosol extinctions larger than the pre-winter values. This is significantly larger than the 25% of water vapor measurements that show a deficit in this temperature bin, suggesting that type I PSCs are contributing to the elevated aerosol extinction. *Nedoluha et al.* [2000] also note the presence of Type I PSCs in June–July of 1998. In Figure 2 the coldest temperatures coincide with the highest aerosol extinction values. All of the observations with $T > 195$ K show low aerosol extinction values, less than 0.001 km^{-1} .

By the August–September viewing period, the distributions of water vapor mixing ratios for all temperature bins with $T < 195$ K peak near 2.2 ppmv. For $195 < T < 210$ K, the majority of the observations are centered around 4 ppmv but there are measurements with mixing ratios less than 3 ppmv in this temperature range as well. The aerosol extinction distributions during

this time have a small percentage of observations with aerosol extinctions above 0.001 km^{-1} and these coincide with the coldest temperatures ($T < 188 \text{ K}$). Thus by this time in the winter, there exists dehydrated air that does not directly coincide with regions of low temperatures or high aerosol extinction values.

Although temperatures at high latitudes are warmer by November, water vapor mixing ratios have recovered only slightly from the dehydration. The distribution for 70°S - 80°S peaks at 3.0 ppmv. While some water vapor recovery has taken place in November, the overall mixing ratios are still substantially below the April mode value (~ 4.3 ppmv) before any dehydration occurred.

3. Extent and Timing of Dehydration

To quantify the horizontal extent of the dehydration, its development throughout the winter months, and its relationship to the areas of cold temperatures, and high aerosol extinction, we calculate the area encompassing the vortex and the regions of low water vapor mixing ratios, high aerosol extinction, and cold temperatures. Criteria for identifying depleted water vapor (mixing ratios less than 3.0 ppmv) and “high” aerosol extinction (larger than 0.001 km^{-1}) are determined empirically from the frequency distributions as described in the previous section (Figure 2). The cold temperature criteria are the ice frost point ($T < 188 \text{ K}$) and the ice nucleation temperature (typically 3 K less than the frost point, $T < 185 \text{ K}$ [Tabazadeh *et al.*, 2000b; Chang *et al.*, 1999]). We use a scaled potential vorticity value of 1.4 s^{-1} to approximate the vortex boundary [Manney *et al.*, 1994; Santee *et al.*, 1998]. Figure 3 shows the calculated daily areas from April through November on the 465 K potential temperature surface. The calculations do not include regions poleward of 80°S due to the latitudinal sampling of the UARS instruments.

The area of temperatures below the frost point of ice begins to develop in mid June. At this time areas with high aerosol extinction are present but there is no evidence of dehydration. The area of high aerosol extinction values diminishes on June 24 and then increases again.

Tabazadeh et al. [2000a] show that denitrification at 450 K occurred over 12 days from about June 12-24. Temperatures below the ice nucleation point are present over a small area in mid June but do not persist or develop over larger areas until after June 27. On July 10, the area of depleted water vapor coincides roughly with both the area of temperatures below the ice nucleation point (185 K) and the area of high aerosol extinction. When water vapor measurements are available again in mid August, the dry area (with water vapor < 3 ppmv) exceeds the cold temperature area (temperature < 188 K) and persists at $\sim 12 \times 10^6$ km² through most of September. *Vömel et al.* [1995] balloon borne measurements in 1994 show that dry water vapor profiles over the McMurdo Station in the Antarctica persist from August to September in agreement with our global analysis of dry water vapor fields in 1992. Cold temperature areas shrink rapidly at the end of August. The area of high aerosol extinction is much less than the dry area during August and September, indicating that severe dehydration has occurred. The only reasonable explanation for this is that the ice clouds have precipitated, irreversibly removing water vapor over a vast area. The dehydrated areas persist and remain at nearly a constant value (from early August to late September) after the area of high aerosol extinction has vanished in early September and after the vortex area begins to recede in early September. From mid August through late September the dehydrated area is roughly 30%-35% of the total vortex area equatorward of 80°S. The dehydrated area decreases rapidly after November 15, and the water vapor values start a rapid recovery. The water vapor mixing ratios at 465 K (Figure 1) increase between mid September and early November, similar to what is observed for nitric acid [*Santee et al.*, 1999]. The dehydrated area in Figure 3 does not show this recovery occurring since the area will not decrease until mixing ratios exceed 3 ppmv, indicating that water vapor values have returned to the levels present prior to the onset of cold temperatures.

4. Model Aerosol Extinctions

Next we focus on the aerosol extinction measurements from CLAES. Previous studies have used these measurements to identify PSCs [Mergenthaler *et al.*, 1997; Ricaud *et al.*, 1995; Massie *et al.*, 1994]. Here we use Mie calculations to compute aerosol extinction due to ice particles. The calculated extinction values are compared to the CLAES observations to infer ice particle size and number density.

Our calculated aerosol extinction depends upon temperatures, pressure, water vapor mixing ratio and fraction of aerosols nucleated into ice particles. To compute the aerosol extinction, we have distributed the volume of condensed water (as ice) at equilibrium over a fixed and assumed number density of ice particles. The size of the ice particles obtained in this manner, for a given number density, were used as input parameters into a Mie code to convert the volume and size information into aerosol extinction units [Toon *et al.*, 1990; Massie *et al.*, 1994]. The CLAES observations are compared with aerosol extinction calculated using different assumptions as to the number density of ice particles based on the range of number densities observed in the in situ data [Hofmann *et al.*, 1991]. Maps of the calculated extinction are formed by computing the aerosol extinction for the temperatures at the geographic locations of the CLAES measurements when the temperature is below the threshold for type II PSCs (188 K). At locations where this temperature criterion is not met, the observed CLAES values are used in constructing the aerosol extinction maps. The maps depict what the CLAES instrument would have observed if type II PSCs were present in the locations where they are predicted to form and if the instrument measured perfectly. We examine days from early in the winter since once condensation and ice particle formation begins, the amount of water vapor available changes. For the early wintertime conditions, we use a mixing ratio of 4.1 ppmv, based on the mean values in Figure 1. Figure 4 shows maps of the CLAES data and calculated aerosol extinction for three different assumptions of ice particle density. The figure shows that an ice particle number density in the range of 10^{-2} - 10^{-3} cm^{-3} best matches the CLAES observations. The comparison between the observed and calculated aerosol extinction is good

despite the uncertainty in the CLAES measurements for high values of aerosol extinction.

The size of ice particles associated with the concentrations of 10^{-2} - 10^{-3} cm^{-3} is shown in Figure 5. The distributions are formed from the calculated sizes for the days in Figure 4. Ice particle sizes are on the order of 10-30 μm . These should be considered general values since the real atmosphere is likely to contain a distribution of ice particle number densities and sizes. In general our inferred ice particle number density is in good agreement with balloon observations over McMurdo station [*Hofmann et al.*, 1991] of ice particle number densities in the range of 10^{-2} to 10^{-3} cm^{-3} .

5. Temperature Statistics

The interpretation of the time development of the area of dehydration compared to the area of cold temperatures (Figure 3) is limited in that it does not include the temperature history of air parcels. In this section, we use temperature statistics from National Centers for Environmental Prediction (NCEP) trajectory calculations to look at the onset of temperatures which meet the ice nucleation conditions for the formation and growth of water ice clouds.

For each day in June through September, 20 points were homogeneously distributed within the 188 K temperature contour at 50 hPa. Twenty forward and backward trajectories were run isentropically from the initialized points for 14 days. Diabatic descent occurs in the Antarctic lower stratosphere at a rate of approximately 35 m/day [*Schoeberl et al.*, 1992]. At this rate, ~ 0.5 km large-scale descent occurs in the vortex over the course of the 14 day trajectory runs. Given that the vertical resolution (3-4 km) of the MLS and CLAES instruments is larger than 0.5 km descent which occurs in 14 days, we neglect the impact of diabatic descent in the trajectory calculations. The statistics of the trajectory analysis are shown in Figure 6. The solid line depicts the percentage of trajectories for each day that have passed through the ice nucleation criterion (reaching temperatures of about 185 K or below). Symbols and error bars show the average and the minimum and maximum time that the ensemble of trajectories spends below the ice frost point (188 K) after the nucleation criterion

has been met.

The temperature statistics obtained from air parcel trajectories suggest that the onset of dehydration occurred at the end of June when a significant number of the trajectories met the nucleation criterion for the formation of ice particles. By early July, 60 to 90% of the parcels encountered temperatures below 185 K, suggesting that by this time ice particles nucleated in nearly all the air parcels initialized within the 188 K temperature contour. Cloud model sensitivity studies show that a $5 \mu\text{m}$ particle can sediment ~ 1 km in just 1 day [Salawitch *et al.*, 1989]. In the previous section we demonstrated that ice particle sizes must have been larger than $5 \mu\text{m}$ to yield aerosol extinction values measured by the CLAES instrument in late June. Thus the lifetime of ice particles nucleated was long enough (5 days or longer) to provide sufficient time for growth and sedimentation of large ice particles ($> 5 \mu\text{m}$) to lower altitudes, causing dehydration.

6. Comparison of dehydration from POAM and MLS

A recent study of water vapor and aerosol extinction data from POAM III examines dehydration in the Antarctic for the SH winter of 1998 [Nedoluha *et al.*, 2000]. POAM is a solar occultation instrument and makes 14 measurements per day in each hemisphere around a latitude circle. The latitude sampled, shown in Figure 7, varies with a semi-annual period. The POAM instrument measures water vapor and aerosol extinction with a high vertical resolution (~ 1 km) in the lower stratosphere, making it useful for studies of dehydration and PSC occurrence. Nedoluha *et al.* [2000] report dehydration occurring over a 6 week period starting in mid July with the drop in water vapor coincident with the timing of the minimum temperatures dropping below the ice frost point in air parcels sampled by the POAM instrument and with the occurrence of a significant number of aerosol extinction measurements indicating the presence of type II PSCs.

While the data used in our study cover a different calendar year, we note that our analysis of the water vapor mixing ratios from MLS and temperature statistics suggests that the onset

of dehydration begins prior to early July, and it is therefore necessary that we relate our conclusions to those of *Nedoluha et al.* [2000]. MLS mixing ratios from 70°S to 80°S drop significantly (from 4 to 2.7 ppmv) from mid June to July 10 (Figure 1). The area of depleted water vapor and cold temperatures begins to develop in late June (Figure 3). *Vömel et al.* [1995] suggest that dehydration and the cold temperature regions develop initially in the interior of the vortex and expand outward. Thus the first observation of dehydrated air depends upon the latitude being sampled. From late June through mid July, the POAM instrument observes latitudes from 65°S-70°S. The MLS water vapor measurements in this latitude range do not show evidence of significant depletion on 10-12 July (Figure 7), whereas a substantial drop in mixing ratio is evident in the MLS data closer to the pole (70°S-80°S) for those dates. Because MLS measurements shows no signs of water vapor loss in mid June and substantial depletion on 10 July, we conclude that the onset of dehydration occurred sometime between mid June and 10 July. Further, temperature statistics provide additional support for the onset of dehydration to be around late June. Therefore, if the meteorological conditions during the 1992 and 1998 Antarctic southern winters are comparable, then the onset of dehydration observed by occultation type instruments will be later than the onset seen by instruments that can view into polar darkness. By August, POAM is observing latitudes poleward of 70°S and deficits in the water vapor are apparent in the data during this period [*Nedoluha et al.*, 2000]. Thus, while the POAM data provides a much finer vertical picture and better continuity than do the MLS data, it is important to note that the latitudinal sampling influences the determination of the onset of dehydration.

7. Summary

Examining satellite measurements of water vapor from the SH winter of 1992, we find evidence for dehydration due to the formation of type II PSCs on potential temperature surfaces from 420 to 520 K (16 to 22 km). However, 1998 POAM observations of water vapor show that dehydration extends down to ~ 360 K (12 km). Thus the vertical extent of

dehydration may have been at least 4 km deeper than what MLS can see, according to the POAM data. The deficits in water vapor are seen in measurements from mid July persisting into November. Mean mixing ratios decrease by approximately 1 to 2 ppmv. Temperature statistics suggest that the onset of dehydration occurs in late June when a large number of cold air mass trajectories meet the ice nucleation criteria. Because the onset of dehydration initially occurs close to the pole, the latitudinal sampling of the atmosphere by different instruments must be taken into account for the determination of the dehydration onset. The development of dehydration over the course of the winter shows that initially (June-July observations) water vapor deficits are found only in areas which have cold temperatures (below 188 K). These areas coincide with those with high aerosol extinction. Area calculations show that regions which meet the cold temperature criteria and those which meet the criteria for dry air expand throughout July. By August, the dry regions are larger than those of the cold temperatures and high aerosol extinction. The depleted mixing ratios persist after the elevated aerosol extinction and cold temperatures diminish. Results from a Mie code calculation in conjunction with the aerosol extinction measurements give a general estimate of aerosol properties. A number density between 10^{-2} - 10^{-3} cm^{-3} best matches the observed aerosol extinction and our estimate of ice particle size is on the order of 10-30 μm .

Acknowledgments. This work is supported by the NASA Upper Atmosphere Research Satellite Program. Work at the Jet Propulsion Laboratory, California Institute of Technology, was done under contract with NASA. Temperature histories used here were obtained from the Goddard Space Flight Center automailer system. We thank Darin Toohey for helpful comments and suggestions.

References

- Bowman, K. B., Large-scale isentropic mixing properties of the Antarctic polar vortex, *J. Geophys. Res.*, pp. 23,013–23027, 1993.
- Browell, E. V., C. F. Butler, S. Ismail, P. A. Robinette, A. F. Carter, N. S. Higdon, O. B. Toon, M. R. Schoeberl, and A. F. Tuck, Airborne lidar observations in the wintertime Arctic stratosphere: Polar stratospheric clouds, *Geophys. Res. Lett.*, *17*, 385–388, 1990.
- Chang, H. A., T. Koop, L. T. Molina, and M. J. Molina, Phase transition in emulsified HNO₃/H₂O and HNO₃/H₂SO₄/H₂O solutions, *J. Phys. Chem.*, *103*, 2673–2679, 1999.
- Hanson, D. H., A. R. Ravishankara, and S. Solomon, Heterogeneous reactions in sulfuric acid aerosols: A framework for model calculations, *J. Geophys. Res.*, *99*, 3615–3629, 1994.
- Hofmann, D. J., and T. Deshler, Stratospheric cloud observations during formation of the Antarctic ozone hole in 1989, *J. Geophys. Res.*, *96*, 2897–2912, 1991.
- Hofmann, D. J., S. J. Oltmans, and T. Deshler, Simultaneous balloon-borne measurements of stratospheric water vapor and ozone in the polar regions, *Geophys. Res. Lett.*, *18*, 1011–1014, 1991.
- Kelly, K. K., et al., Dehydration in the lower Antarctic stratosphere during late winter and early spring, *J. Geophys. Res.*, *94*, 11317–11357, 1989.
- Kent, G. S., C. R. Trepte, U. O. Farrukh, and M. P. McCormick, Variation in the stratospheric aerosol associated with the north cyclonic polar vortex as measured by the SAM II satellite sensor, *J. Atmos. Sci.*, *42*, 1536–1551, 1985.
- Manney, G. L., R. W. Zurek, A. O'Neill, and R. Swinbank, On the motion of air through the stratospheric polar vortex, *J. Atmos. Sci.*, *51*, 2973–2994, 1994.
- Manney, G. L., R. Swinbank, S. T. Massie, M. E. Gelman, A. J. Miller, R. Nagatani, A. O'Neill, and R. W. Zurek, Comparison of U. K. Meteorological Office and U. S. National Meteorological Center stratospheric analyses during northern and southern winter, *J. Geophys. Res.*, *101*, 10311–10334, 1996.

- Manney, G. L., Y. J. Orsolini, H. C. Pumphrey, and A. E. Roche, The 4-day wave and transport of UARS tracers in the austral polar vortex, *J. Atmos. Sci.*, *55*, 3456–3470, 1998.
- Manney, G. L., H. A. Michelsen, M. L. Santee, M. R. Gunson, F. W. Irion, A. E. Roche, and N. J. Livesey, Polar vortex dynamics during spring and fall diagnosed using trace gas observations from the Atmospheric Trace Molecule Spectroscopy instrument, *J. Geophys. Res.*, *104*, 18841–18866, 1999.
- Massie, S. T., D. Baumgardner, and J. E. Dye, Estimation of polar stratospheric cloud volume and area densities from UARS, stratospheric aerosol measurement II, and polar ozone and aerosol measurement II extinction data, *J. Geophys. Res.*, *103*, 5773–5783, 1998.
- Massie, S. T., et al., Spectral signatures of polar stratospheric clouds and sulfate aerosol, *J. Atmos. Sci.*, *51*, 3027–3044, 1994.
- Massie, S. T., et al., Simultaneous observations of Polar Stratospheric Clouds and HNO₃ over Scandinavia in January, 1992, *Geophys. Res. Lett.*, *24*, 595–598, 1997.
- Mergenthaler, J. L., J. B. Kumer, A. E. Roche, and S. T. Massie, Distribution of antarctic polar stratospheric clouds as seen by the CLAES experiment, *J. Geophys. Res.*, *102*, 19161–19170, 1997.
- Nedoluha, G. E., R. M. Bevilacqua, K. W. Hoppel, M. Daehler, E. P. Shettle, J. H. Hornstein, M. D. Fromm, J. D. Lumpe, and J. E. Rosenfield, POAM III measurements of dehydration in the Antarctic lower stratosphere, *Geophys. Res. Lett.*, *27*, 1683–1686, 2000.
- Pierce, R. B., W. L. Grose, J. M. Russell III, A. F. Tuck, R. Swinbank, and A. O'Neill, Spring dehydration in the Antarctic stratospheric vortex observed by HALOE, *J. Atmos. Sci.*, *51*, 2931–2941, 1994.
- Pumphrey, H. C., Validation of a prototype water vapor retrieval for UARS MLS, *J. Geophys. Res.*, *104*, 9399–9412, 1999.
- Pumphrey, H. C., H. L. Clark, and R. S. Harwood, Lower stratospheric water vapor measured by UARS MLS, *Geophys. Res. Lett.*, *27*, 1691–1694, 2000.

- Randall, C. E., et al., An overview of POAM II aerosol measurements at 1.06 μm , *Geophys. Res. Lett.*, 23, 3195–3198, 1996.
- Ricaud, P. D., et al., Polar stratospheric clouds as deduced from MLS and CLAES measurements, *Geophys. Res. Lett.*, 22, 2033–2036, 1995.
- Rosen, J. M., D. J. Hofmann, J. R. Carpenter, J. W. Harder, and S. J. Oltmans, Balloon-borne Antarctic frost point measurements and their impact on polar stratospheric cloud theories, *Geophys. Res. Lett.*, 15, 859–862, 1988.
- Rosenlof, K. H., A. F. Tuck, K. K. Kelly, J. M. Russell III, and M. P. McCormick, Hemispheric asymmetries in water vapor and inferences about transport in the lower stratosphere, *J. Geophys. Res.*, 102, 13,213–13,234, 1997.
- Salawitch, R. J., G. P. Gobbi, S. C. Wofsy, and M. B. McElroy, Denitrification in the Antarctic stratosphere, *Nature*, 339, 525–527, 1989.
- Santee, M. L., W. G. Read, J. W. Waters, L. Froidevaux, G. L. Manney, D. A. Flower, R. F. Jarnot, R. S. Harwood, and G. E. Peckham, Interhemispheric differences in polar stratospheric HNO_3 , H_2O , ClO and O_3 , *Science*, 267, 849–852, 1995.
- Santee, M. L., A. Tabazadeh, G. L. Manney, R. J. Salawitch, L. Froidevaux, W. G. Read, and J. W. Waters, UARS Microwave Limb Sounder HNO_3 observations: Implications for Antarctic polar stratospheric clouds, *J. Geophys. Res.*, 103, 13285–13313, 1998.
- Santee, M. L., G. L. Manney, L. Froidevaux, W. G. Read, and J. W. Waters, Six years of UARS Microwave Limb Sounder HNO_3 observations: Seasonal, interhemispheric, and interannual variations in the lower stratosphere, *J. Geophys. Res.*, 104, 8225–8246, 1999.
- Schoeberl, M. R., L. R. Lait, P. A. Newman, and J. E. Rosenfield, The structure of the polar vortex, *J. Geophys. Res.*, 97, 7859–7882, 1992.
- Solomon, S., Stratospheric ozone depletion: A review of concepts and history, *Rev. Geophys.*, 37, 275–316, 1999.
- Tabazadeh, A., M. L. Santee, M. Y. Danilin, H. C. Pumphrey, P. A. Newman, P. J. Hamill, and

- J. L. Mergenthaler, Quantifying denitrification and its effect on ozone recovery, *Science*, 288, 1407–1411, 2000a.
- Tabazadeh, A., S. T. Martin, and J. S. Lin, The effect of particle size and nitric acid uptake on the homogeneous freezing of aqueous sulfuric acid particles, *Geophys. Res. Lett.*, 27, 1111–1114, 2000b.
- Thomason, L. W., and L. R. Poole, Use of stratospheric aerosol properties as diagnostics of Antarctic vortex processes, *J. Geophys. Res.*, 98, 23003–23012, 1993.
- Toon, O. B., P. Hamill, R. P. Turco, and J. Pinto, Condensation of HCl and HNO₃ in the winter polar stratosphere, *Geophys. Res. Lett.*, 13, 1284–1287, 1986.
- Toon, O. B., E. V. Browell, S. Kinne, and J. Jordan, An analysis of lidar observations of polar stratospheric clouds, *Geophys. Res. Lett.*, 17, 393–396, 1990.
- Vömel, H., S. J. Oltmans, D. J. Hofmann, T. Deshler, and J. M. Rosen, The evolution of the dehydration in the Antarctic stratospheric vortex, *J. Geophys. Res.*, 100, 13919–13926, 1995.
- WMO, Scientific assessment of ozone depletion: 1998, Rep. 44, 1999.

H. C. Pumphrey, Department of Meteorology, The University of Edinburgh, Edinburgh UK EH9 3JZ

Michelle Santee, Jet Propulsion Laboratory, 4800 Oak Grove Drive, MS 183-701, Pasadena, CA 91109-8099.

Eric Jensen and Elizabeth M. Stone and Azadeh Tabazadeh, Mail Stop 245-4, NASA Ames Research Center, Moffett Field, CA

John L. Mergenthaler, Lockheed Martin Advanced Technology Center, 3251 Hanover Street, Palo Alto, California 94304

Figure Captions

Figure 1. Daily mean MLS water vapor mixing ratios (ppmv) in black and CLAES aerosol extinction (km^{-1}) in grey for 70°S - 80°S . Data are from April 1992 - March 1993 and have been interpolated to potential temperature surfaces.

Figure 2. Frequency distributions of MLS water vapor (per 0.1 ppmv increment) on the left and CLAES aerosol extinction data (increments of 1.0 km^{-1}) times the power of ten on the log axis) on the right at the 465 K potential temperature surface. Measurements from 50°S - 80°S are binned by temperature. The black curve represents data from 70°S - 80°S (all temperatures). The distributions are compiled from the data available in the UARS southern-viewing periods.

Figure 3. Area (in km^2) in the SH equatorward of 80°S at 465 K which is composed of vortex air (black); of mixing ratios less than 3.0 ppmv representing dry air (black circles); aerosol extinction larger than 0.001 km^{-1} (grey circles); temperatures less than 185 K (dotted line); temperatures less than 188 K (dashed line). The regions of low water vapor, high aerosol extinction, and cold temperature are constrained to be inside the vortex.

Figure 4. CLAES extinction and calculated extinction for three different number densities at 465 K. The white contours show temperature (195, 188, and 185 K).

Figure 5. Size distribution of the particles from the calculated aerosol extinction for the days depicted in Figure 4 and for number densities of 10^{-2} and 10^{-3} cm^{-3} .

Figure 6. Temperature statistics of air mass trajectories. Twenty forward and backward isentropic trajectories were run each day from points homogeneously distributed within the 188 K temperature contour at 50 hPa. The solid line depicts the percentage of the trajectories for each day which have had temperatures less than 185 K in their trajectory; circles and error bars indicate the average and the maximum and minimum time the trajectory stayed below 188 K after the 185 K nucleation criterion was met.

Figure 7. Daily mean MLS water vapor mixing ratios averaged over two latitude ranges: 70°S - 80°S (black) and 65°S - 70°S (grey) for April-September 1992. Dashed line depicts the POAM tangent point latitude.

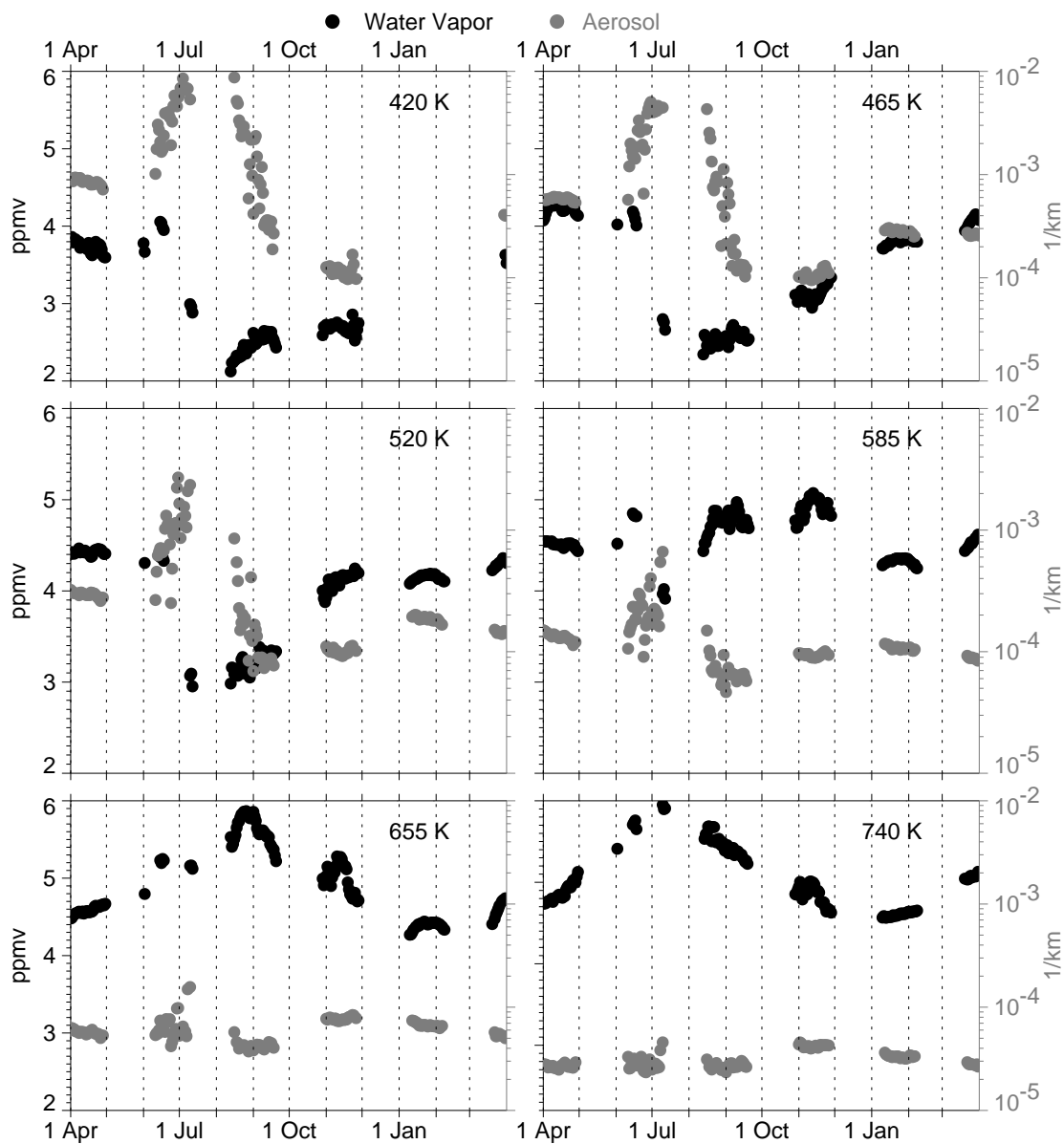


Figure 1. Daily mean MLS water vapor mixing ratios (ppmv) in black and CLAES aerosol extinction (km^{-1}) in grey for 70°S - 80°S . Data are from April 1992 - March 1993 and have been interpolated to potential temperature surfaces.

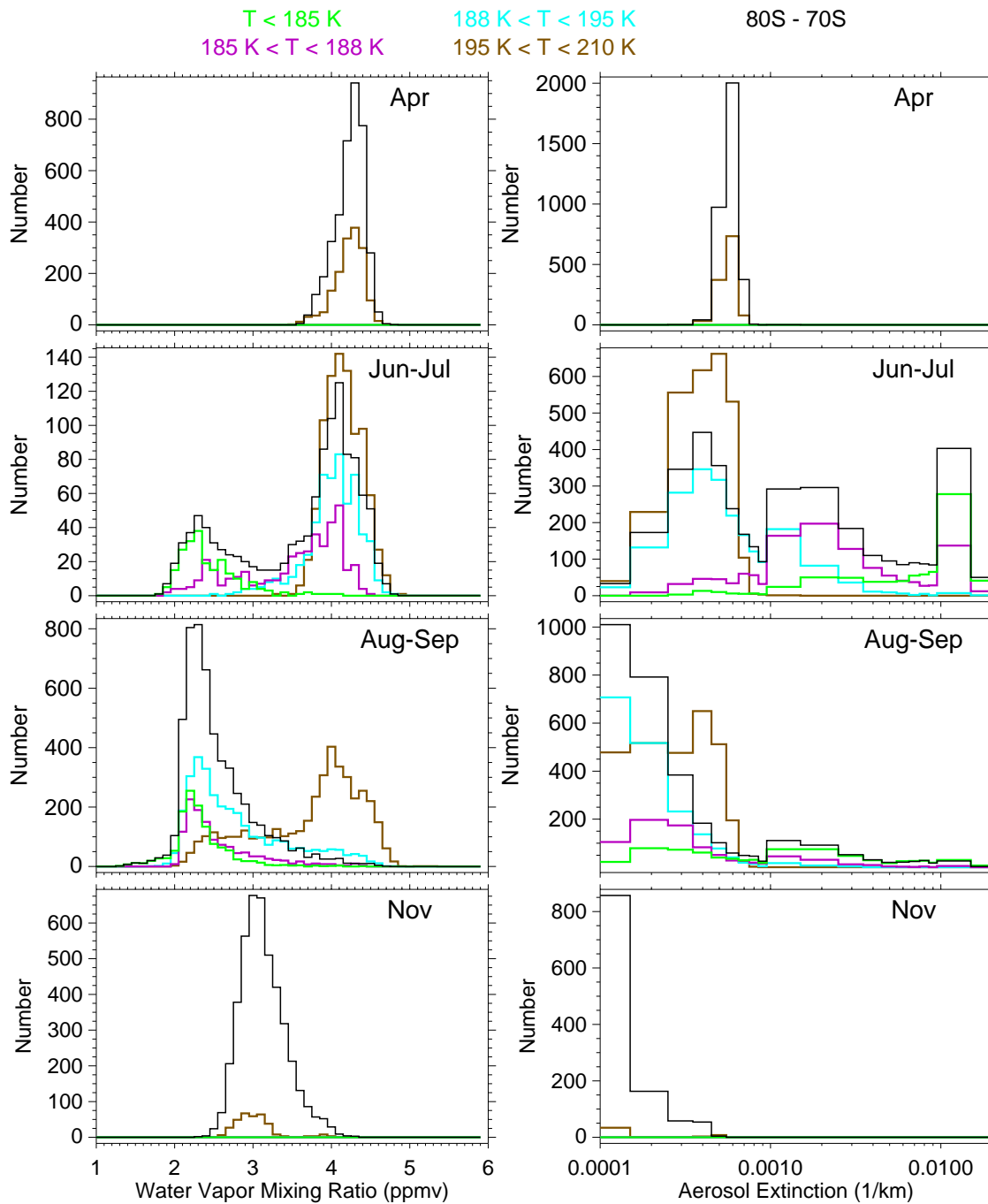


Figure 2. Frequency distributions of MLS water vapor (per 0.1 ppmv increment) on the left and CLAES aerosol extinction data (increments of 1.0 km^{-1}) times the power of ten on the log axis) on the right at the 465 K potential temperature surface. Measurements from 50°S - 80°S are binned by temperature. The black curve represents data from 70°S - 80°S (all temperatures). The distributions are compiled from the data available in the UARS southern-viewing periods.

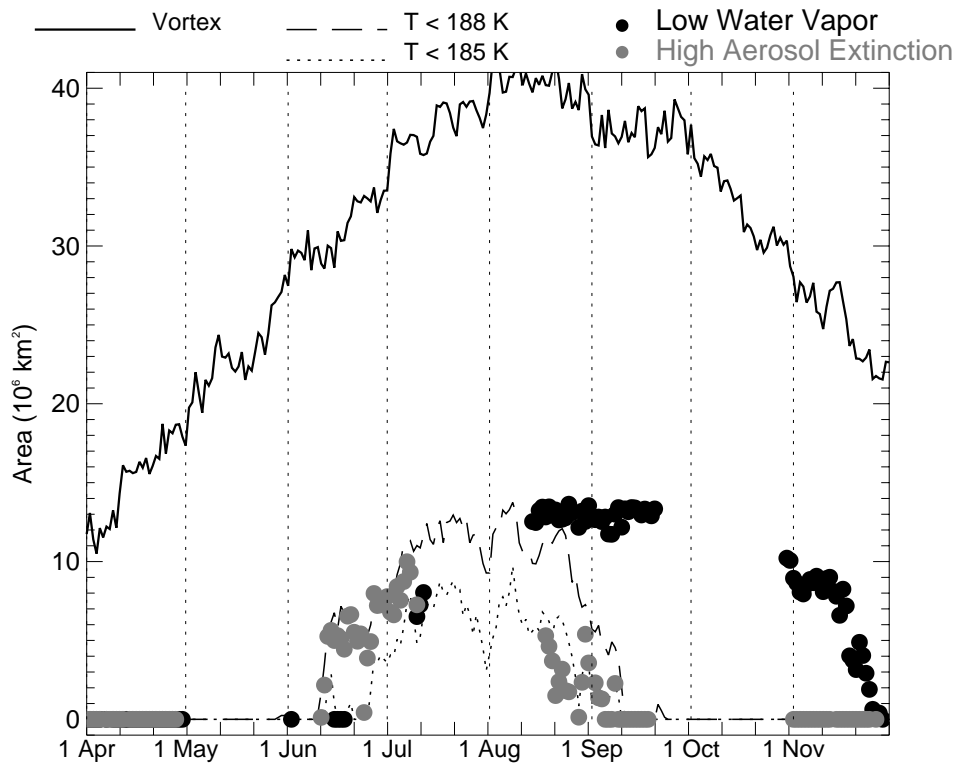


Figure 3. Area (in km^2) in the SH equatorward of 80°S at 465 K which is composed of vortex air (black); of mixing ratios less than 3.0 ppmv representing dry air (black circles); aerosol extinction larger than 0.001 km^{-1} (grey circles); temperatures less than 185 K (dotted line); temperatures less than 188 K (dashed line). The regions of low water vapor, high aerosol extinction, and cold temperature are constrained to be inside the vortex.

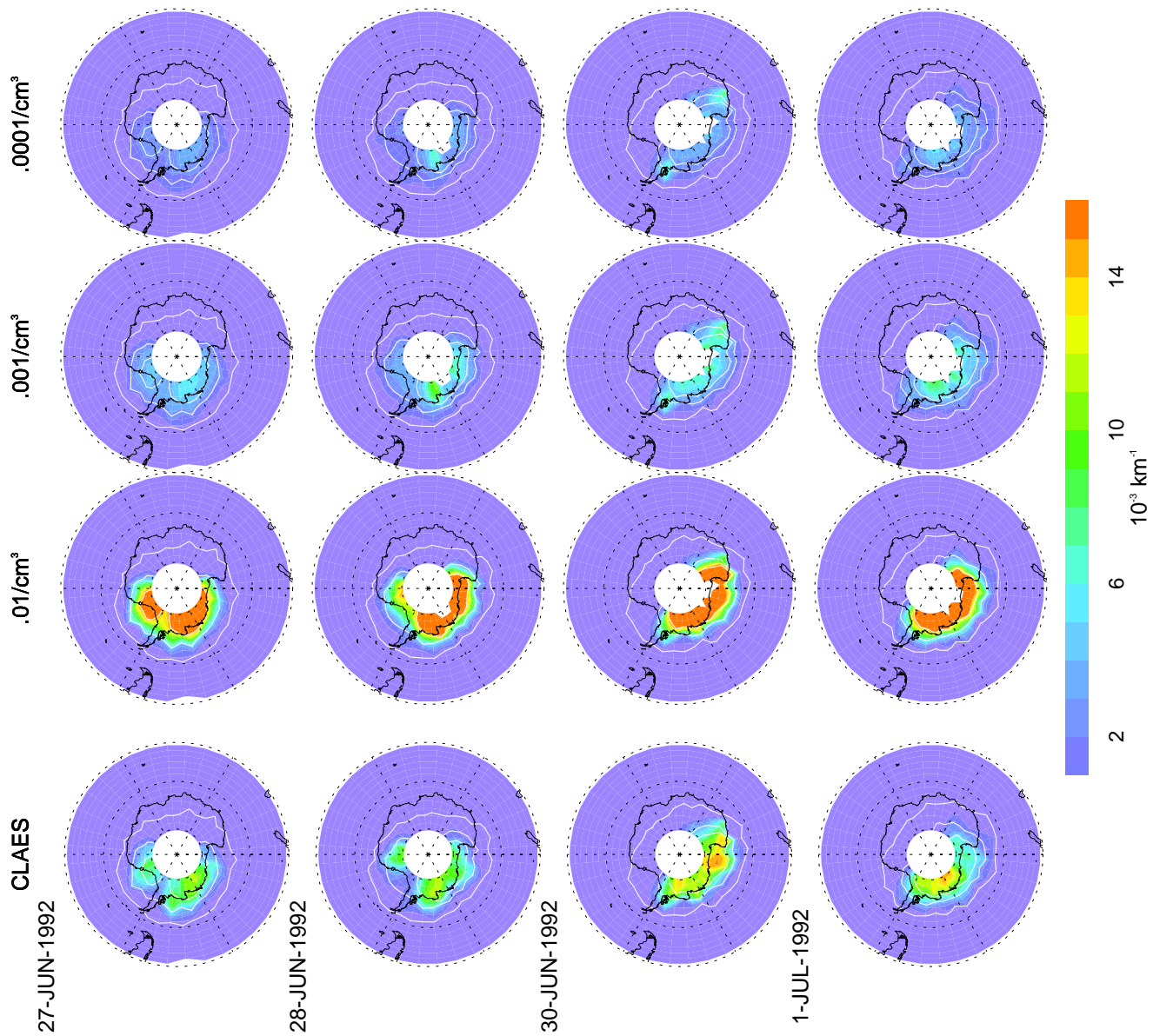


Figure 4. CLAES extinction and calculated extinction for three different number densities at 465 K. The white contours show temperature (195, 188, and 185 K).

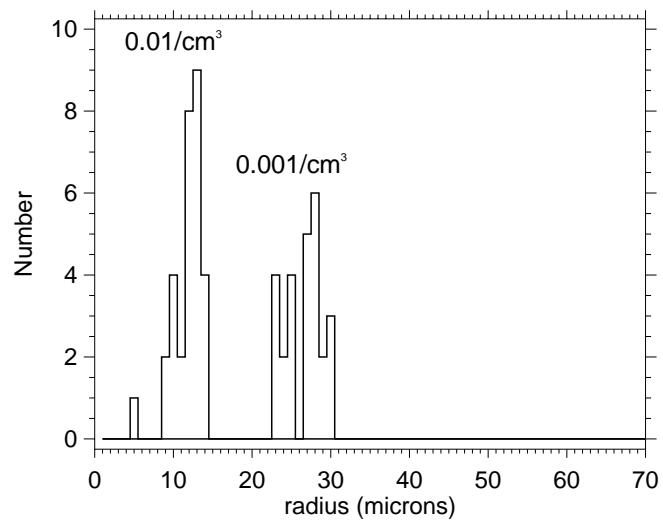


Figure 5. Size distribution of the particles from the calculated aerosol extinction for the days depicted in Figure 4 and for number densities of 10^{-2} and 10^{-3} cm^{-3} .

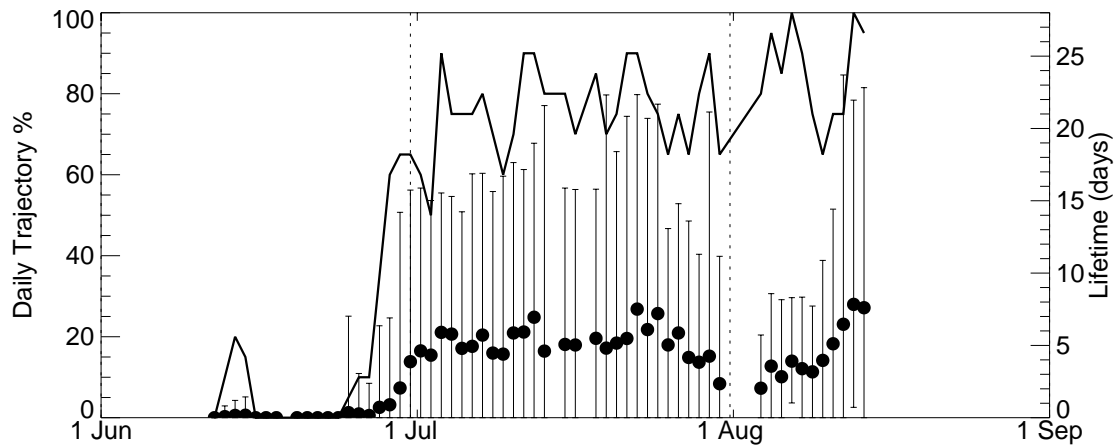


Figure 6. Temperature statistics of air mass trajectories. Twenty forward and backward isentropic trajectories were run each day from points homogeneously distributed within the 188 K temperature contour at 50 hPa. The solid line depicts the percentage of the trajectories for each day which have had temperatures less than 185 K in their trajectory; circles and error bars indicate the average and the maximum and minimum time the trajectory stayed below 188 K after the 185 K nucleation criterion was met.

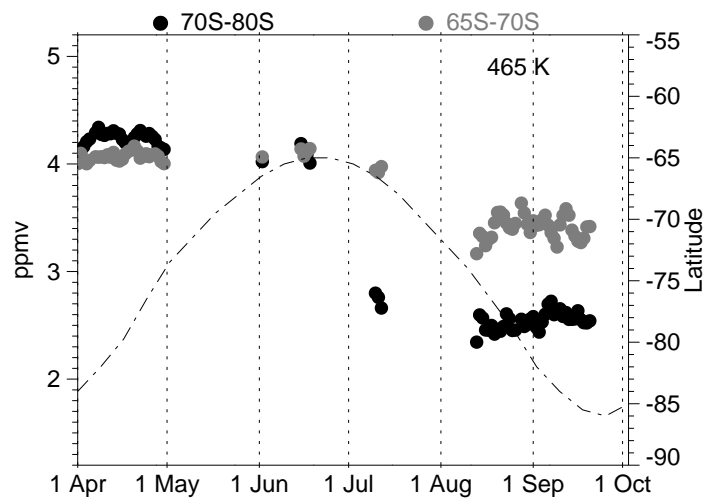


Figure 7. Daily mean MLS water vapor mixing ratios averaged over two latitude ranges: 70°S-80°S (black) and 65°S-70°S (grey) for April-September 1992. Dashed line depicts the POAM tangent point latitude.